Electronic Supplementary Material (ESI) for Dalton Transactions.
This journal is © The Royal Society of Chemistry 2014

Green synthesis of Fe_3O_4 nanoparticles with controlled morphology using urease and their application in dye adsorption

Haitang Shi,[ab] Longfei Tan,[a] Qijun Du,[a] Xue Chen,[ab] Linlin Li,[a] Tianlong Liu,[a] Changhui Fu,[a] Huiyu Liu[a] and Xianwei Meng*[a]

[a] Laboratory of Controllable Preparation and Application of Nanomaterials, Research Center for Micro&Nano Materials and Technology, Technical Institute of Physics and Chemistry, Chinese Academy of Sciences, Beijing 100190, People's Republic of China. E-mail: mengxw@mail.ipc.ac.cn; Fax: +86-10-62554670; Tel: +86-10-82543521

[b] University of Chinese Academy of Sciences, Beijing 100049, People's Republic of China.

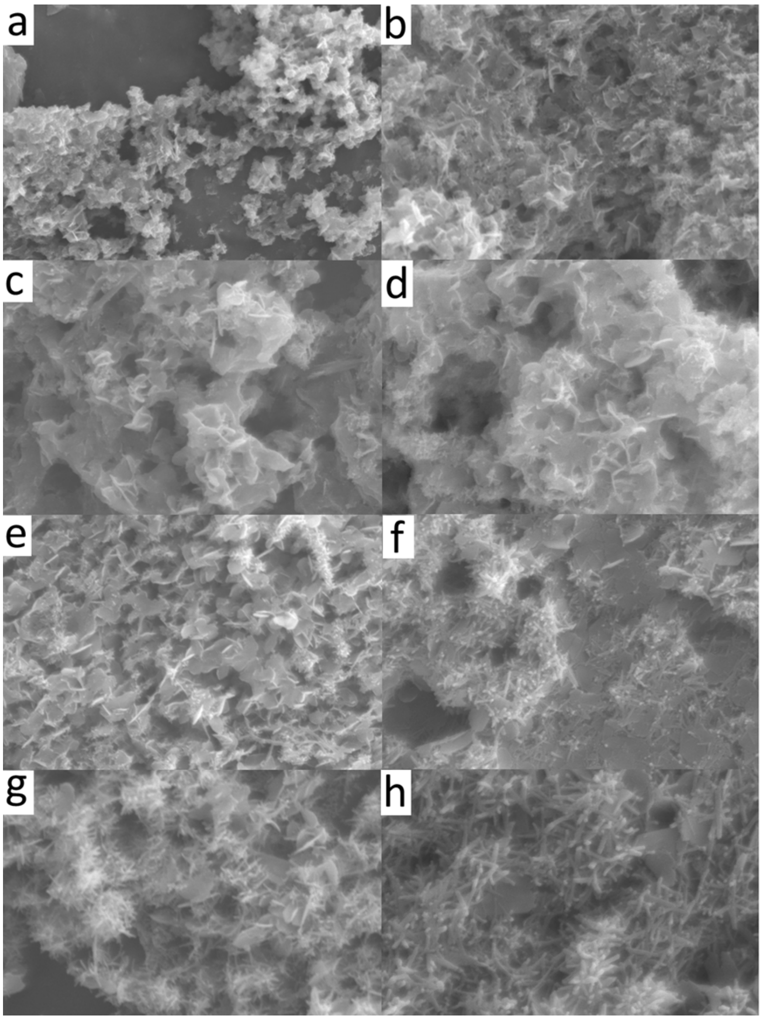

Figure S1. SEM images of Fe_3O_4 nanoparticles of 15 min (a), 30 min (b), 45 min (c), 60 min (d) at 40 ℃, and 75 min (e), 90 min (f), 105 min (g), 120 min (h) at 60 ℃.

To explore the formation mechanism of nanosheets and nanorods, the kinetics of the reaction was investigated in detail through SEM analysis as in Figure S1. The reaction was kept at 40 ℃ for an hour and 60 ℃ for another hour. The former four pictures show that when the reaction temperature was kept at 40 ℃, the Fe_3O_4 nanosheets and nanorods nucleus appear simultaneously. Through visual observation, large amounts of nanosheets are in sight with larger size compared with nanorods. When the reaction continues and the temperature rises to 60 ℃, the nanorods become predominant over the nanosheets with the size growing larger as shown in later four pictures. The situation for nanosheets is just on the contrary. Comprehensive analyse these pictures at different temporal points, we can obtain the summary that competitive growth of Fe_3O_4 nanorods and nanosheets at different temperature results in the formation of different morphologies (High temperature is good for the growth of Fe_3O_4 nanorods and low temperature for Fe_3O_4 nanosheets). These pictures at different temporal points provide more insights on the shape evolution of the nanoparticles.

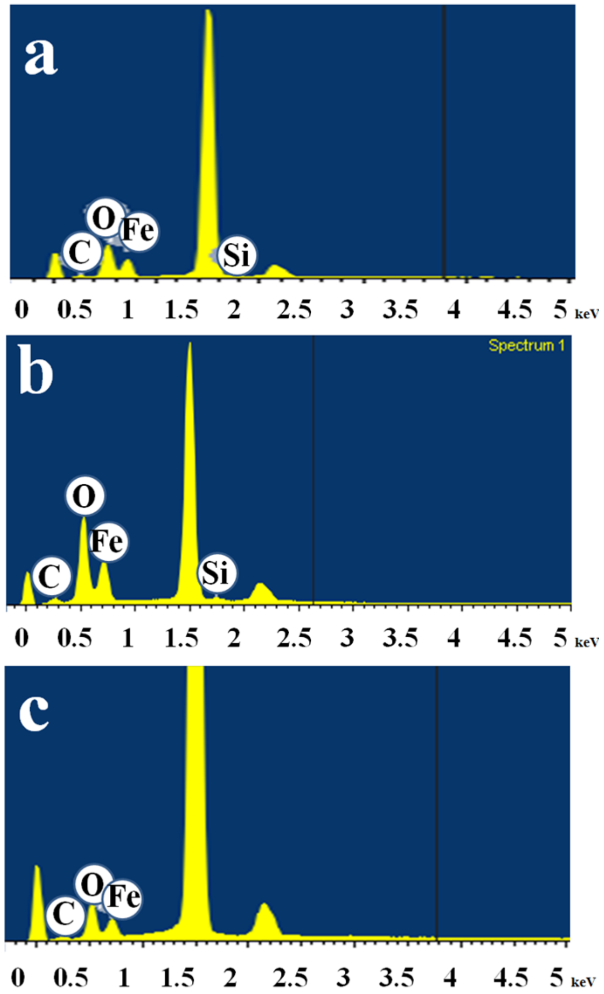

Figure S2. EDX images of Fe_3O_4 nanospheres (a), nanosheets (b) and nanorods (c).

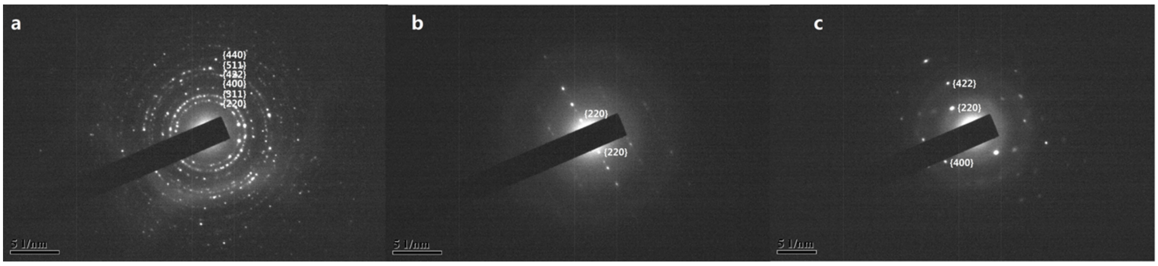

Figure S3. SAED images of Fe_3O_4 nanospheres (a), nanosheets (b) and nanorods (c).

We have obtained images of the selected area electron diffraction (SAED) by focusing the electron beams perpendicular to the basal plane of individual Fe_3O_4 nanoparticles. The polycrystalline rings can be observed clearly from the image of the Fe_3O_4 nanospheres. Due to the influence of urease and different reaction temperature, the growth along different crystal direction is significantly different. For the Fe_3O_4 nanosheets, the majority of large sheets grow along the {220} planes by adsorption small particles, whereas Fe_3O_4 nanorods can grow along different directions, including the {220}, {400}, {422} planes.

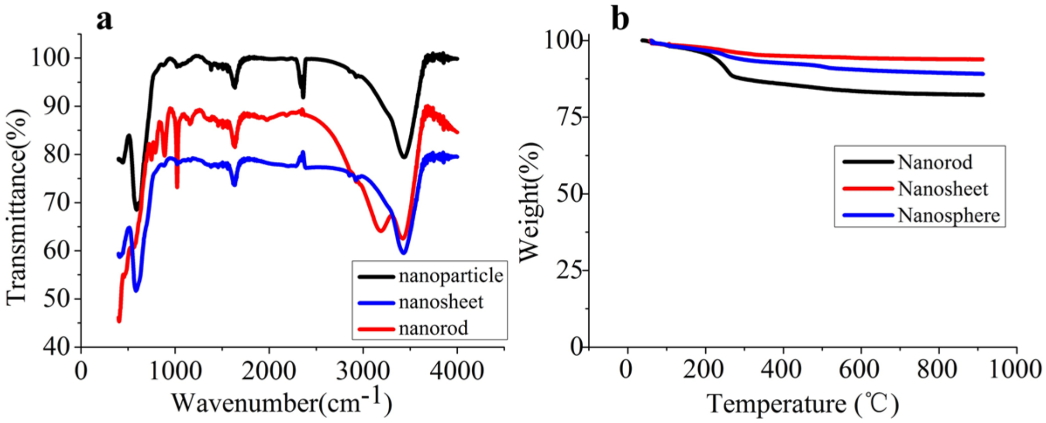

Figure S4. (a) FT-IR spectra, and (b) TGA curve of Fe_3O_4 nanoparticles.

Fourier transform infrared spectra are applied to analysis the chemical nature of the nanoparticles. Figure S4a shows the spectrum of Fe_3O_4 nanoparticles in various morphologies, indicating that for these three kinds of nanoparticles, the peaks displayed at 590 cm^{-1} corresponding to the Fe-O vibration relates to the magnetite phase.

In order to further confirm the composition of the as-prepared nanoparticles, we have measured the thermograms of Fe_3O_4 samples with various morphologies through thermogravimetric analysis in the temperature range from room temperature to 900 °C with a heating rate of 10 °C per minute in the air flow. The curves in Figure S4b show initially a negligible weight loss below 100 °C, which confirms the loss of hydrogen bonded water molecule present at the surface of samples. A second obvious weight loss occurred around the temperature range of 200 °C, which is probably due to the removal of trapped water molecules from the lattice, as well as the removal of amino groups or redundant urease adsorbed on the surface of samples. The total weight loss of the three kinds of Fe_3O_4 nanoparticles are 6.17%, 10.92% and 17.71% for nanosheets, nanospheres and nanorods, respectively. The difference value of weight loss may primarily be caused by the different adsorption percent of water molecules.

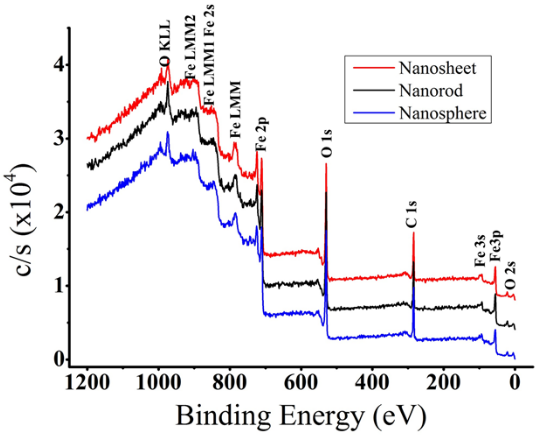

Figure S5. Full XPS spectra of Fe_3O_4 nanoparticles.

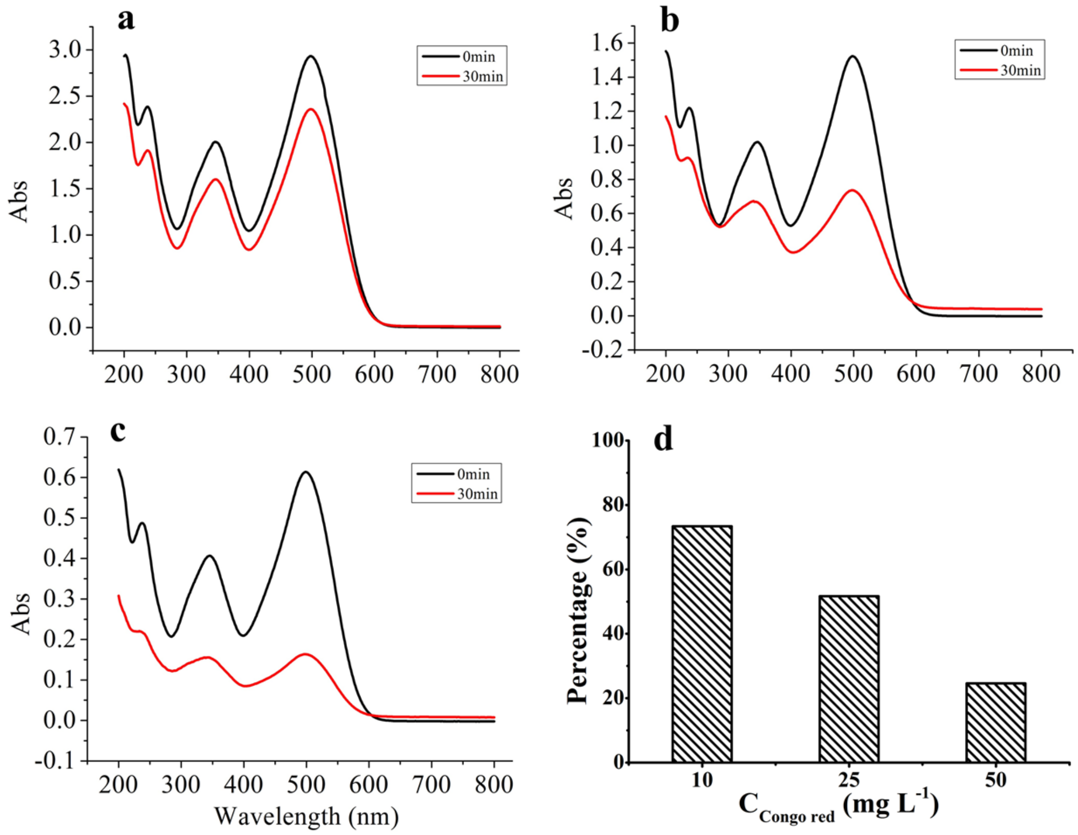

Figure S6. UV-Vis spectrophotometer spectrum of Congo red with the initial concentration of 50 mg L^{-1} (a), 25 mg L^{-1} (b) and 10 mg L^{-1} (c) in the presence of equivalent Fe_3O_4 nanoparticles, (d) comprehensive analysis results of the adsorption results of a~c.

To study the optimum initial concentration of Congo red, different groups of parallel adsorption experiment were designed. In each experimental group, Congo red with the initial concentration range from 10 to 50 mg L^{-1} was used. The quality of Fe_3O_4 nanoparticles was equivalent in each group. The UV-Vis spectrophotometer spectrum was measured at the same time point of the adsorption process. As in Figure S6, with the increase of the concentration of Congo red, the difference between the peak value decreases. When the concentration of Congo red is as low as 10 mg L^{-1}, the adsorption percentage can reach the maximum value of 73.40 % with the adsorption capacity of 3.67 mg g^{-1}. Congo red with lower concentration was suitable to be measured with UV-Vis and the concentration of 25 and 10 mg L^{-1} were chosen to make detail time-depending analysis, which was shown in Figure S7.

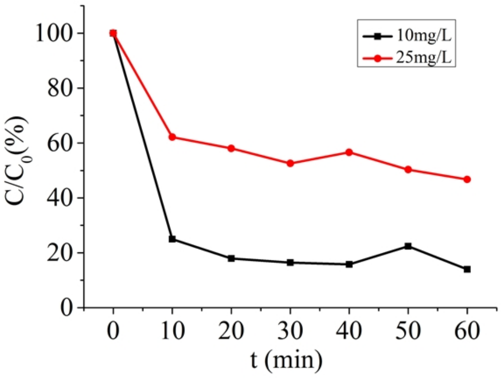

Figure S7. Adsorption results of Congo red with different initial concentrations by Fe_3O_4 nanoparticles.

Figure S7 compares the adsorption results of Congo red with the initial concentrations of 25 and 10 mg L^{-1}. With the time extension, the concentration of Congo red, *C*, is decreasing slowly. In 10~15 min, the adsorption rate of Congo red can reach the maximum and when time is longer than 10 min, the adsorption rate gradually slows down. The situation is similar for the two experiment group, but the maximum adsorption capacity of Congo red become different for high and low concentration. This may be related to the relative amount of Fe_3O_4 nanoparticles and Congo red, and the concentration of 10 mg L^{-1} was chosen to be discussed in this paper to study the adsorption capacity of Fe_3O_4 nanoparticles.

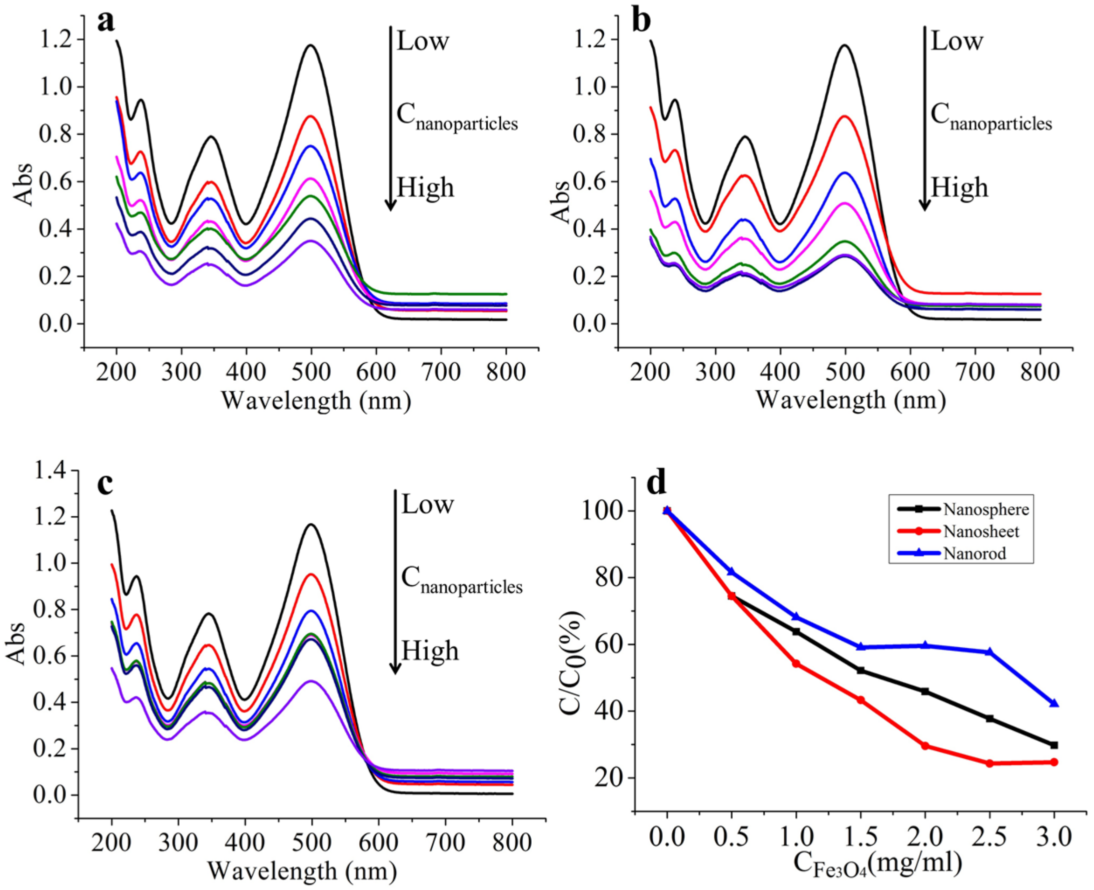

Figure S8. UV-Vis spectrophotometer spectrum of Congo red in the presence of Fe_3O_4 nanospheres (a), nanosheets (b) and nanorods (c) with different concentrations, comprehensive analysis results of Fe_3O_4 nanoparticles with different concentrations (d).

To study the relationship between the adsorption percent and concentration of Fe_3O_4 nanoparticles, the adsorption experiments were designed as below, the Fe_3O_4 nanoparticles with different concentrations were used as adsorbent and parallel adsorption experiment was taken as shown in Figure S8. For Fe_3O_4 nanoparticles, including nanospheres, nanosheets and nanorods, with the increasing of the concentration, the adsorption percent increases obviously. Figure S8d compares the adsorption results of Congo red adsorbed by Fe_3O_4 nanoparticles in various morphologies, which can also clearly demonstrate that Fe_3O_4 nanosheets own better adsorption capacity of Congo red, regardless of which concentration value level. This result is consistent with time-depending result in Figure 5a of main text.

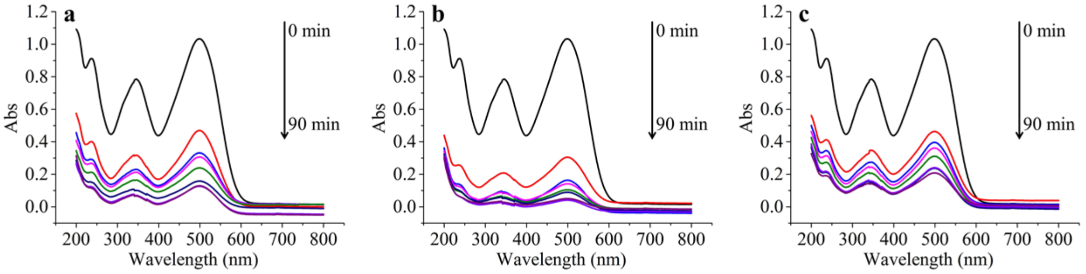

Figure S9. UV-Vis spectrophotometer spectrum of Congo red in the presence of Fe_3O_4 nanospheres (a), nanosheets (b) and nanorods (c) in different adsorption times.

For Fe_3O_4 nanospheres, nanosheets and nanorods, the UV-Vis spectrum in different adsorption times follows a similar regulation. Comparing the spectrum at 0 min with that of 10, 20, 30, 40, 50 and 60 minutes, we can observe that the intensity of the Congo red characteristic peaks all decreases gradually. In 10~15 min, the adsorption rate of Congo red can reach the maximum and when time is longer than 10 min, the adsorption rate gradually slows down.